Case (vi): $M \neq 0$, $\lambda = 0$, $n = 0$

The velocity components in the case of steady Hele-Shaw flow of viscous, incompressible conducting fluid are

$$u = \frac{A}{M}\left[1 - \frac{\cos i\,(M/\nu)^{\frac{1}{2}} z}{\cos i\,(M/\nu)^{\frac{1}{2}} d}\right]\left[1 - \frac{a^2(x^2 - y^2)}{(x^2 + y^2)^2}\right] \tag{2.29}$$

$$v = -\frac{A}{M}\left[1 - \frac{\cos i\,(M/\nu)^{\frac{1}{2}} z}{\cos i\,(M/\nu)^{\frac{1}{2}} d}\right]\left[\frac{2a^2 xy}{(x^2 + y^2)^2}\right]. \tag{2.30}$$

Case (vii): $M = 0$, $\lambda = 0$, $n = 0$

The velocity components in the case of steady Hele-Shaw flow of viscous incompressible fluid are

$$u = \frac{A(h^2 - z^2)}{2\nu}\left[1 - \frac{a^2(x^2 - y^2)}{(x^2 + y^2)^2}\right] \tag{2.31}$$

$$v = -\frac{A(h^2 - z^2)}{2\nu}\left[\frac{2a^2 xy}{(x^2 + y^2)^2}\right]. \tag{2.32}$$

3. Conclusions

We have investigated the effects of magnetic parameter M and the relaxation time λ on the velocity components u and v. In Fig. 1 the velocity component u is plotted against z for different values of M. It is clear from this figure that the velocity component u decreases with the increase in magnetic parameter M. Figure 2 shows the effect of relaxation time λ on velocity component u. We observe that u decreases with the increase in λ. In Fig 3 $-v$ is drawn against z for different values of M and for different values of λ in Fig. 4. We notice that the velocity component v increases as M or λ increases. We have derived velocity components u and v in different cases.

1. Buckmaster, J., *J. Fluid Mech.*, 1970, **41**, 523.
2. Lamb, H., *Hydrodynamics*, 6th edition, 1932, Art. p. 330.
3. Lee, J. S. and Fung, Y. C., *J. Fluid Mech.*, 1969, **31**, 657.
4. Sparrow, E. M. and Cess, R. D., *J. Appl. Mech.*, 1962, **29**, 181.
5. Swaminathan, K., *Ph.D. Thesis*, Agra University, 1975.
6. Thompson, B. W., *J. Fluid, Mech.*, 1968, **31**, 379.

PALYNOLOGICAL STUDIES ON SOME LIVERWORTS OF GARHWAL HIMALAYAS

M. P. SHARMA, R. P. RATURI AND R. D. GAUR
Department of Botany, Garhwal University, Srinagar 246 174, *India*

Abstract

The present communication pertains to the study of 20 species belonging to 13 genera of the order Anthocerotales and Marchantiales. Diversity in sporomorphs was noticed. The exine usually protrudes into various types of processes, *i.e.*, verrucose, spinulose, spinose and gemmulate and represents various peculiar ornamentation such as foveolate, punctate and reticulate, indicating their distinctiveness. Perine and triradiate ridge may be present or absent.

Introduction

ALTHOUGH palynology has recently received due attention, there are only a few reports on the bryophytes. Our knowledge on the spores of bryophytes is mainly confined the general morphology and taxonomy of the group. Historical account on the spore study of bryophytes is given by Udar[1]. However, some of the important contributions on different aspects were made by McClymont[2], Terasmae[3], Tallis[4], Erdtman[5] and others.

Perusal of earlier literature indicates great need for the study on spore morphology. The authors have made an attempt to study the spore morphology of some of the common liverworts collected from Garhwal Himalayas at the elevation range of 700–2000 m.

Materials and Methods

Spore preparations were made by Erdtman's acetolysis method[6] and most of the terms used in the text follow the pattern as proposed by Erdtman. The specimens and slides are maintained in the Palynology Laboratory, Botany Department, Garhwal University, Srinagar.

Observations

Anthoceros erectus Kash.—Spores ± spheroidal, amb circular, average diameter 29·6 μ, range 28–31 μ, triradiate ridge distinct, exine reticulate protruding into verrucose processes of 3·17 μ (Fig. 1).

A. himalayensis Kash.—Spores ± spheroidal, amb circular, average diameter 31 μ, range 28–34 μ, triradiate ridge prominent, exine reticulate, LO-pattern (Figs. 2*a*, *b*).

A. chambensis Kash.—Spores ± spheroidal, average diameter 26 μ, range 24–29 μ, triradiate ridge distinct, exine reticulate with warty margins.

Notothylas indica Kash.—Spores ± spheroidal, average diameter 29 μ, range 26–31 μ, exine thick, aerolate and producing baculae of 5·6 μ, perine pre ent (Figs. 3*a*, *b*).

N. levieri Schiff.—Amb triangular, average size 35 μ, range 30–40 μ, triradiate ridge distinct reaching upto periphery, exine thin (Fig. 4).

Dimortiera hirsuta Rein. Bl. et Nees.—Spores ± spheroidal, amb triangular, average size 70 μ, range 60–78 μ, exine spinose, occasionally baculate, perine present (Figs. 5*a*, *b*, *c*).

Marchantia palmata Nees.—Spores in tetrads, individual spores ± spheroidal, size 42 μ, range 39 45 μ, exine thin, without any distinct processes, granulose (Figs. 6*a*, *b*, *c*).

Targionia hypophylla Linn.—Spores ± spheroidal, average size 52 μ, range 48–56 μ, triradiate ridge not distinct, exine reticulate, LO, OL-pattern, exine verrucate, perine absent (Figs. 7*a*, *b*, *c*).

Cyathodium tuberosum Kash.—Spores tetrahedral, average size 70 μ, range 60–78 μ, exine 3 μ thick, spinose, spines pointed, perenium well developed (Figs. 8*a*, *b*).

Plagiochasma articulatum Kash.—Spores ± spheroidal, amb circular, average size 59 μ, range 53–65 μ, exine 3 μ thick with baculate processes (Figs. 9*a*, *b*, *c*, *d*).

P. intermedium Linn. et G.—Spores ovate spheroidal, size 57·5 μ, range 52–62 μ, triradiate mark quite distinct, reaching upto periphery, exine thin, aerolate (Fig. 10).

P. simlensis Kash.—Spores spheroidal, amb wavy and round, average size 46·5 μ, range 43–50 μ, exine reticulate, perenium present (Figs. 11*a*, *b*).

Athalmia pinguis Falc.—Spores globose, amb triangular, average size 83 μ, range 78–90 μ, exine thin, warty with obtuse papillae, deeply reticulate, perenium present (Figs. 12*a*, *b*).

Fimbriaria angusta St.—Spores tetrahedral, amb triangular, average size 77 μ, range 71–84 μ, triradiate mark distinct, exine 3 μ thick, reticulate, perenium distinct (Figs. 13*a*, *b*).

F. blumeana Nees.—Spores ovate spheroidal, average size 83 μ, range 78–87 μ, exine reticulate with large luminae, perenium present (Figs. 14*a*, *b*).

F. reticulata Kash.—Spores ± spheroidal, amb circular, average size 65 μ, range 60–70 μ, exine punctate, perenium present (Figs. 15*a*, *b*).

Exormotheca tuberifera Kash.—Spores ± spheroidal, amb wavy, average size 61·7 μ, range 57–67 μ, exine rugulate, perenium obscure (Figs. 16*a*, *b*).

Cryptometrium himalayense Kash.—Spores tetrahedral amb triangular, size 85 μ, range 78–90 μ, triradiate ridge well marked, exine papillate, perine present (Fig. 17).

Conocephalum conicum (Linn.) Neckers—Spores ± spheroidal, average size 29 μ, range 25–31 μ, triradiate ridge ill-marked, exine slightly wavy with small warts, perine present (Figs. 18*a*, *b*).

Reboulia hemispherica (Linn.) Raddi.—Spores tetrahedral, average size 65·5 μ, range 62–69 μ, exine 3 μ thick, spinose, perenium present (Figs. 19*a*, *b*).

Discussion

Spore morphology of liverworts shows different pecularies and the exine surface represents various patterns of ornamentation. The sporomorph of investigated species are marked by variation in shape, size, exine ornamentation and processes, including triradiate mark and perenium.

Spores in all the species of Anthocerotales except in *Notothylas levieri* (tetrahedral) are ± spheroidal. Size of the spores ranges from 24 μ (*Anthoceros chambensis*) to 49 μ (*Notothylas levieri*). Distinct triradiate ridge is presented by all the spores except *Notothylas indica*.

Spores in Marchantiales are varying in shape from tetrahedral to spheroidal. In *Marchantia palmata* some of the spores remain united in tetrads. Smallest size of spores (25 μ) was noticed in *Conocephalum conicum* and largest (90 μ) in *Athalmia pinguis* and *Cryptometrium himalayense*. Triradiate ridge is obscure in most of the species. An interesting feature represented by these spores is the presence of perine with folded margins, however, *Marchantia palmata*, *Plagiochasma articulatum*, *P. intermedium*, and *P. simlensis* are the exceptions. The species of *Fimbriaria* are distinct in their exine features, *i.e.*,

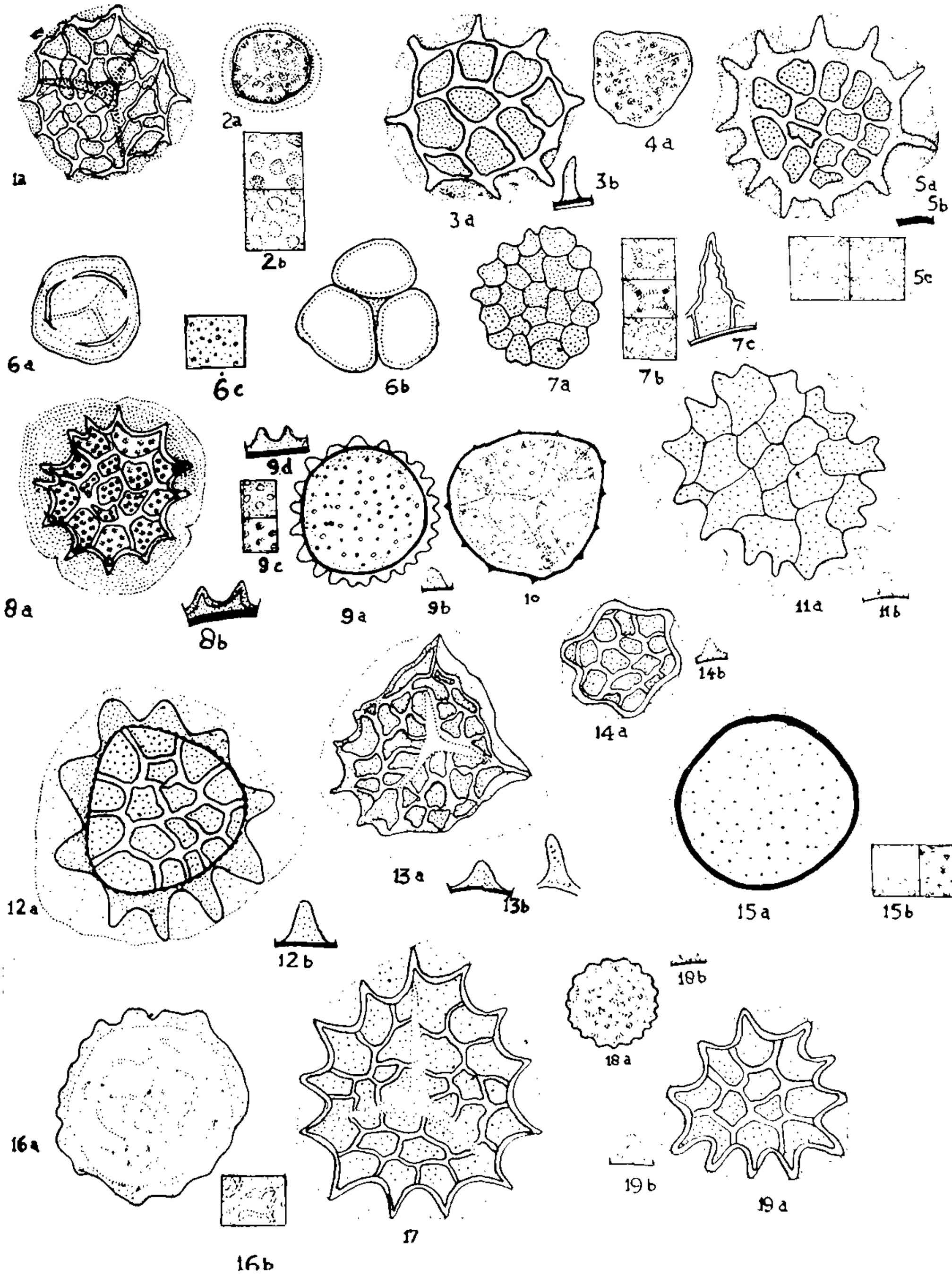

FIGS. 1–19. Fig. 1. *Anthoceros erectus.* Fig. 2*a*. *A. himalayensis*. Fig. 2*b*, LO-pattern. Fig. 3*a*. *Notothylas indica*. Fig. 3*b*. Bacula. Fig. 4. *N. levieri*. Fig. 5*a*. *Dumortiera hirsuta*. Fig. 5*b*. Bacula. Fig. 5*c*. Exine surface. Fig. 6*a*. *Marchantia palmata*. Fig. 6*b*. Spore tetrad. Fig. 6*c*. Exine surface. Fig. 7*a*. *Targionia hypophylla*. Fig. 7*b*. Surface. Fig. 7*c*. Spine. Fig. 8*a*. *Cyathodium tuberosum*. Fig. 8*b*. Spine. Fig. 9*a*. *Plagiochasma articulatum*. Fig. 9*b*. Bacula. Fig. 9*c*. LO-pattern. Fig. 9*d*. Process. Fig. 10. *Plagiochasma intermedium*.

Fig. 11*a*. *P. sinlensis*. Fig. 11*b*. Exine process. Fig. 12*a*. *Athalmia pinguis*. Fig. 12*b*. Process. Fig. 13*a*. *Fimbriaria angusta*. Fig. 13*b*. Process. Fig. 14*a*. *F. blumeana*. Fig. 14*b*. Exine. Fig. 15*a*. *F. reticulata*. Fig. 15*b*. LO-pattern. Fig. 16*a*. *Exormotheca tuberifera*. Fig. 16*b*. Surface pattern. Fig. 17. *Cryptometrium himalayense*. Fig. 18*a*. *Conocephalum conicum*. Fig. 18*b*. Exine. Fig. 19*a*. *Reboulia hemispherica*. Fig. 19*b*. Exine. (All figures × 450; Fig. representing LO 1000.)

F. angusta (reticulate with papillae). *F. blumeana* (reticulate with large lumina). *F. reticulata* (punctate). Exine with papillae of different sizes and blunt ends is represented by *Plagiochasma articulatum*, *P. intermedium*, *Athalmia pinguis*, *Conocephalum conicum* and *Reboulia hemispherica*. Out of three species of *Plagiochasma* studied only *P. intermedium* bears a distinct triradiate mark.

ACKNOWLEDGEMENTS

This work was supported by financial assistance from University Grants Commission, New Delhi, for which one of us (RDG) is thankful.

1. Udar, R., In *Advances in Palynology*, ed. by P. K. K. Nair, National Botanic Gardens, Lucknow, 1964, 79–100.
2. McClymont, *Bryologist*, 1955, **58**, 287.
3. Terasmae, J., *Ibid.*, 1955, **58**, 306.
4. Tallis, J. H., *Trans. Br. Bryol. Soc.*, 1962, **4**, 209.
5. Erdtman, G., *Pollen and Spore Morphology and Plant Taxonomy. Gymnosperm, Pteridophyta, Bryophyta*, Stockholm, 1957.
6. —, *Pollen Morphology and Plant Taxonomy, Angiosperms*, Stockholm, 1952.

GLASS MICROSLIDE AS A THERMAL NEUTRON FLUENCE METER

H. S. SAINI, A. P. SRIVASTAVA AND G. RAJAGOPALAN
Birbal Sahni Institute of Palaeobotany, 53, University Road, Lucknow 226 007, India

ABSTRACT

Analysis of the spatial distribution of U^{235} induced fission tracks in ordinary glass microslides reveals that they can be used for integrated thermal neutron fluence measurement over many orders of magnitude. Fission events are induced in U^{235} atoms occurring as natural impurities in the glass slides by irradiation with thermal neutrons in Apsara nuclear reactor. The etching of fission tracks and the measurements of track density variation, both in area and depth of the samples, have indicated a uniform and equal distribution of uranium in the slides. The microslides have been calibrated against NBS SRM962 fission track standard glass and GE-Fisher glass. The uranium content in the microslides has been found to be 0·5 ppm. The value for inter-laboratory calibration constant B has been determined as $1·53 \times 10^{11}$ neutrons per track.

INTRODUCTION

FLEISCHER *et al.*[1] have used earlier the sodalime GE-Fisher glass with a calibrated uranium content of 0·35 ppm as a thermal neutron fluence meter in F–T dating. F–T standard glasses were later prepared by many workers[2–5]. At present, various methods exist for the determination of neutron dose given to a material in a nuclear reactor[6] but fission track (F–T) glass fluence meter is one of the cheapest and most accurate. Though small quantities of these standard glasses can be purchased from US National Bureau of Standards yet to use them on a large scale and on routine basis, to study the spatial variation of thermal neutron fluence in a capsule, one needs large quantities. Hence the necessity arises to calibrate a glass standard available in large quantities.

The basic criteria to be satisfied for dosimetric purposes are that the material (preferably glass) should have uranium as an impurity at a concentration level of 0·01 to 500 ppm and it should be uniformly distributed in the volume. A box of Blue Star Super Deluxe microslides manufactured by Polar Industrial Corporation, Bombay, was investigated for using it as a uranium standard glass fluence meter. These microslides are routinely used in optical microscopy for mounting samples before scanning. They are optically plane, highly transparent and are of uniform thickness.